Environmental TEM investigation of the reduction of α-Fe_2O_3 nanorods under H_2 atmosphere

Trevor P. Almeida[1], Michael W. Fay[2], Yanqiu Zhu[3], Thomas W. Hansen[4], Rafal Dunin-Borkowski[4,5] and Paul D. Brown[1*]

[1]Division of Materials, Mechanics and Structures, Department of Mechanical, Materials and Manufacturing Engineering, Faculty of Engineering; &
[2]Nottingham Nanotechnology and Nanoscience Centre;
University of Nottingham, University Park, Nottingham, NG7 2RD, UK.
[3]College of Engineering, Mathematics and Physical Sciences, University of Exeter, Streatham Campus, Exeter, EX4 4QF, UK.
[4]Center for Electron Nanoscopy, Technical University of Denmark, DK-2800 Kgs. Lyngby, Denmark.
[5]Ernst Ruska-Centre for Microscopy and Spectroscopy with Electrons, Institute for Microstructure Research, Research Centre Jülich, D-52425 Jülich, Germany.

Abstract. The thermal reduction of hydrothermally synthesised α-Fe_2O_3 nanorods (NRs) to Fe_3O_4 NRs under hydrogen is investigated. Complete reduction of α-Fe_2O_3 NRs to Fe_3O_4 NRs was achieved during *in situ* XRD under 1 bar H_2 atmosphere at 360ºC. Complementary environmental transmission electron microscope investigation at high resolution, during *in situ* heating under an H_2 pressure of 5 mbar at 500ºC, provided evidence for the very first stages of transformation, supporting a model for the migration of oxygen along favoured α-Fe_2O_3 lattice planes during the templated thermal reduction of α-Fe_2O_3 NRs to Fe_3O_4 NRs.

1. Introduction

One-dimensional (1D) nanostructures have attracted considerable attention due to their novel magnetic properties which are greatly dependent on nanostructure size and shape [1]. Ferrimagnetic magnetite (Fe_3O_4) is of particular interest as a multifunctional nanostructured material with potential application in ferrofluids, magnetic recording and magnetic resonance imaging [2]. Acicular hematite (α-Fe_2O_3) nanorods (NRs) may be used as a precursor for the synthesis of Fe_3O_4 NRs, through a process of partial reduction [3]. Hydrothermal synthesis (HS) constitutes an ideal method for the production of α-Fe_2O_3 NRs from dilute iron (III) chloride ($FeCl_3$) precursor solution, via the formation of an intermediate β-FeOOH (akaganeite) phase. The addition of phosphate anions has been shown to play a decisive role in the anisotropic growth of α-Fe_2O_3 NRs, defining their acicular shape by mediating the process of oriented attachment of primary α-Fe_2O_3 nanoparticles (NPs) [4]. X-ray diffractometry (XRD) investigation of α-Fe_2O_3 NRs heated *in situ* under a reducing atmosphere may be used to gain insight into the process of bulk phase transformation to Fe_3O_4. However, in order to elucidate the intricate details of this phase transformation process, it is necessary to visualise the reduction process at high resolution. Spherical aberration (C_S) correction combined with environmental TEM (ETEM) enables the detailed investigation of localised chemical reactions under gas atmospheres with interpretable spatial resolution at the sub-angstrom level [5, 6]. In this context, a high resolution ETEM investigation of the partial reduction of α-Fe_2O_3 NRs to Fe_3O_4 under conditions of high temperature and reducing atmosphere is presented.

*Author to whom correspondence should be addressed: paul.brown@nottingham.ac.uk

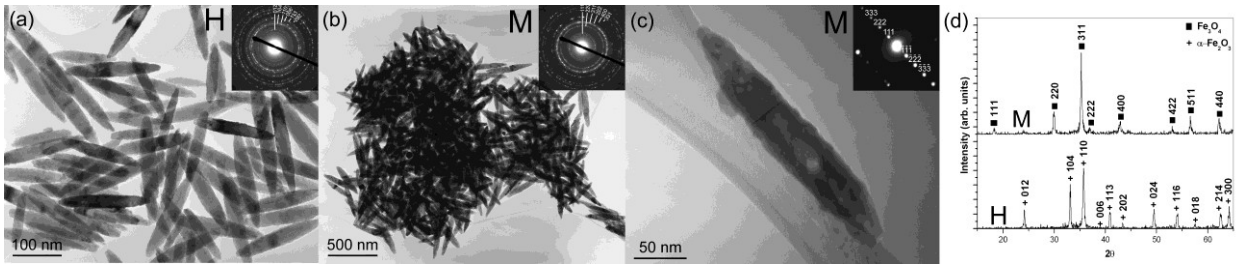

Figure 1 (a-c) BF diffraction contrast TEM images of: (a) α-Fe_2O_3 NRs (Sample H) formed from the HS of 0.2 ml $FeCl_3$ at 200ºC for 2 hours in the presence of 3 mg $NH_4H_2PO_4$, with indexed SAED (inset); (b,c) Fe_3O_4 NRs (Sample M) formed following the annealing of Sample H at 360ºC under ~ 1 bar H_2 atmosphere for 30 min, with indexed SAED (inset). (d) Associated XRD patterns of Samples H and M, indexed to α-Fe_2O_3 (JCPDS 72-469) and Fe_3O_4 (JCPDS 88-315), respectively.

2. Experimental

Acicular α-Fe_2O_3 NRs (Sample H) were prepared through the hydrothermal synthesis of 0.2 ml $FeCl_3$ aqueous solution (45% pure $FeCl_3$; Riedel-de Haen, Germany) in the presence of ammonium dihydrogen-phosphate (99.999% $NH_4H_2PO_4$; Sigma-Aldrich, UK) surfactant, further diluted in 40 ml distilled water and mechanically stirred in a 125 ml Teflon-lined steel autoclave. The autoclave was sealed and inserted into a temperature controlled furnace at a reaction temperature of 200˚C for 2 hours. The autoclave, once removed from the furnace, was allowed to cool down to room temperature naturally. For the purpose of *in situ* XRD investigation, the HS product suspensions were centrifuged for 6 minutes at 6000 rpm, cleaned with acetone, deposited onto single crystal silicon substrates and analysed using a Bruker D8 Advance X-ray diffractometer (Cu Kα radiation; θ/2θ diffraction geometry). Sample H was examined at room temperature and then heated to 360ºC in a sealed XRD sample chamber under an H_2 atmosphere of 1 bar for 30 min (Sample M). For the purpose of TEM investigation, the centrifuged HS and XRD reaction product samples were cleaned with acetone and dispersed using an ultrasonic bath before deposition onto carbon film / gold mesh support grids (Agar Scientific Ltd, UK). Conventional diffraction contrast bright field (BF) imaging of the reaction products was performed using a JEOL 2000FX electron microscope. Further, ETEM investigation of the reduction of Sample H as a function of temperature (room temperature to 500˚C at 20˚C / min under 5 mbar H_2 atmosphere) was performed using a Gatan double tilt heating holder within a FEI Titan E-Cell TEM with a C_S corrector on the objective lens, operated at 300 kV (Centre for Electron Nanoscopy (CEN), Technical University of Denmark). High angle annular dark field (HAADF) imaging was performed using a FEI Titan (S)TEM with a C_S corrector on the condenser system, operated at 300 kV (CEN).

3. Results

The BF diffraction contrast TEM images of Figures 1a-c illustrate the morphology of the initial HS reaction products (Sample H) and the products formed following annealing at 360ºC under ~ 1 bar H_2 atmosphere for 30 min during *in situ* XRD investigation (Sample M). The associated XRD patterns of Samples H and M (Figure 1d) are consistent with the presence of crystalline α-Fe_2O_3 (JCPDS 72-469) and Fe_3O_4 (JCPDS 88-315), respectively. TEM investigation of Sample H (Figure 1a) confirmed the initial HS suspension to comprise acicular α-Fe_2O_3 NRs (~ 420 nm long, ~ 60 wide nm), whilst Sample M (Figures 1b,c) consisted of similar sized acicular Fe_3O_4 NRs.

The heating of Sample H under a reducing atmosphere in the ETEM provided insight into the progressive reduction of α-Fe_2O_3 on the localised scale. No change occurred after 30 min at 360ºC, as seen during *in situ* XRD, and hence the temperature was increased to 500ºC, with a view to accelerate the reduction process. Figure 2 presents BF diffraction and phase contrast TEM images of Sample H acquired at 500ºC under an H_2 atmosphere of 5 mbar. The BF TEM image of Figure 2a shows large α-Fe_2O_3 NRs located near the edge of the gold TEM grid. The phase contrast image of Figure 2b illustrates the fine details of an individual α-Fe_2O_3 NR surface (Figure 2a, boxed region), as identified by (d_{104} = 2.70Å) (inset). Selected images from a time-lapse series acquired at 500˚C provided evidence for the localised development of an Fe_3O_4 NP on the α-Fe_2O_3 NR surface (Figures 2c−i), as evidenced by the {220} (d_{220} = 2.96Å) and {111} (d_{111} = 4.83Å) lattice fringes (Figures 2e & f). Figure 2j shows the newly

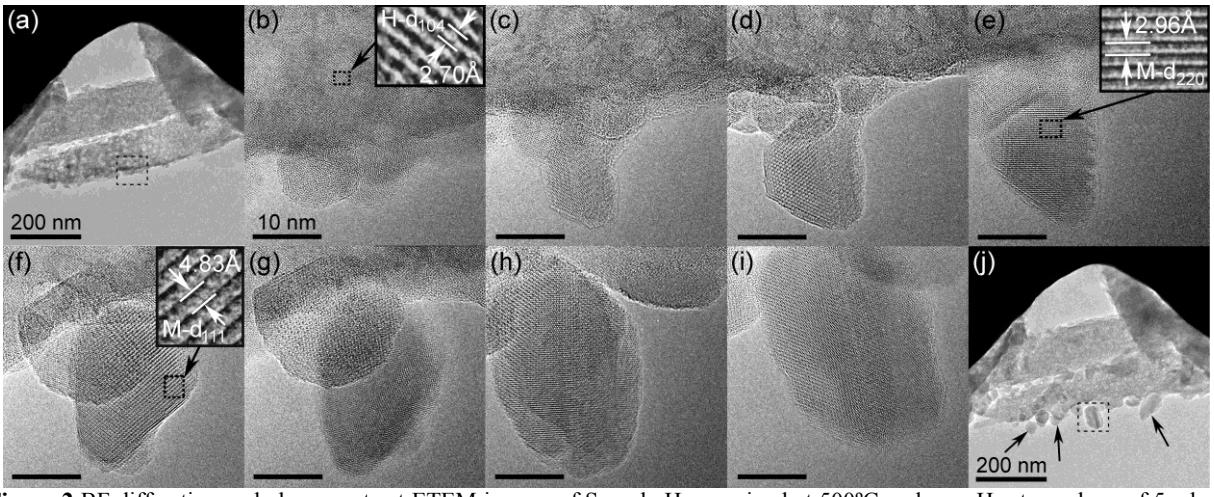

Figure 2 BF diffraction and phase contrast ETEM images of Sample H, examined at 500ºC under an H_2 atmosphere of 5 mbar. (a) Large α-Fe_2O_3 NRs located at the edge of the gold TEM grid. (b) High resolution image of the surface of an α-Fe_2O_3 NR (boxed region of Figure 2a). (c-i) Time-lapse phase contrast images showing the development of an Fe_3O_4 NP, as identified by lattice fringes (e,f inset). Scale bars correspond to 10 nm. (j) α-Fe_2O_3 NRs decorated with the developed Fe_3O_4 NPs (arrowed).

developed Fe_3O_4 NP (outlined) and reveals the presence of additional Fe_3O_4 NPs (arrowed) developed on the α-Fe_2O_3 NR surface during heat treatment.

Figure 3 similarly presents phase contrast ETEM images from Sample H acquired at 500ºC under an H_2 atmosphere of 5 mbar. Figure 3a presents a close examination of the tip of an α-Fe_2O_3 NR, as identified by {104} lattice fringes (d_{104} = 2.70Å) (inset). The defects in the α-Fe_2O_3 NR are an effect of the coalescence of α-Fe_2O_3 particles during growth [4]. Figures 3b,c show the localised development of an Fe_3O_4 NP (arrowed), as identified by {220} lattice fringes (d_{220} = 2.96Å, Figure 3c, inset).

Figure 4 presents BF diffraction contrast and HAADF images of Sample H acquired after 5 hours of heating under a reducing atmosphere within the ETEM. The BF TEM of Figure 4a shows a single crystalline α-Fe_2O_3 NR (~ 420 nm long, ~ 70 nm wide), as identified by SAED (inset). Figures 4b & 4c present HAADF images of α-Fe_2O_3 NRs before and after heating in the ETEM, respectively, with a porous structure of the annealed α-Fe_2O_3 NR revealed in Figure 4c.

4. Discussion

In situ heating of α-Fe_2O_3 NRs in the XRD at 360ºC under an H_2 atmosphere of 1 bar for 30 minutes promoted their complete transition to Fe_3O_4. This is consistent with the reduction of precursor α-Fe_2O_3, being a recognised method for the production of Fe_3O_4, as summarised by the equation: $3Fe_2O_3 + H_2 \rightarrow 2Fe_3O_4 + H_2O$. The H_2 atmosphere interacts with the oxygen of the α-Fe_2O_3 NR surfaces to form water, whilst heating to 360ºC provides sufficient thermal energy to promote oxygen diffusion from inside the α-Fe_2O_3 NRs to restore the equilibrium oxygen concentration at the surface, resulting in partial reduction to Fe_3O_4. SAED combined with TEM imaging of individual NRs showed that the major axes of the α-Fe_2O_3 (Figure 4a) and Fe_3O_4 NRs (Figure 1c) were $<006>_H$ and $<111>_M$, respectively. This orientation relationship between α-Fe_2O_3 and Fe_3O_4 is consistent with previous reduction studies, with oxygen considered to migrate along {006} planes [7]. Here, the restacking to Fe_3O_4 is not so severe as to affect the NR acicular morphology (Figure 1c), hence, the α-Fe_2O_3 NRs act as templates for the topotactic transformation to Fe_3O_4 NRs.

BF TEM imaging and SAED (Figure 4a) during ETEM investigation demonstrated that α-Fe_2O_3 NRs were only reduced to Fe_3O_4 at the NR surfaces, under an H_2 atmosphere of 5 mbar at 500ºC for 5 hours, with the caveat that the achievable H_2 pressure of 5 mbar in ETEM was significantly lower than the 1 bar used during *in situ* XRD investigation. This low H_2 pressure was found to be insufficient to promote the thermal reduction of complete α-Fe_2O_3 NRs during *in situ* heating in the ETEM. Thermal effects, however, did lead to the development of porosity in the α-Fe_2O_3 NRs through the release of trapped water and phosphate [8], as revealed by HAADF imaging (Figure 4c). Nevertheless, it is recognised that the time-lapse imaging at 500ºC during ETEM provided for direct observation of the very first stages of

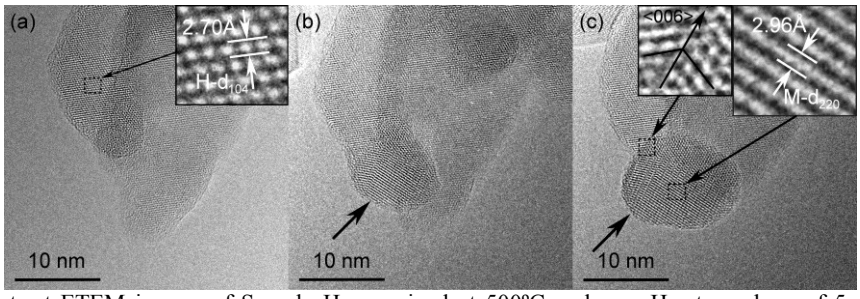

Figure 3 Phase contrast ETEM images of Sample H, examined at 500ºC under an H_2 atmosphere of 5 mbar. (a) Tip of an individual α-Fe_2O_3 NR, identified by lattice fringes (inset). (b,c) Time-lapse images showing the development of an Fe_3O_4 NP, identified by lattice fringes in (c) (inset).

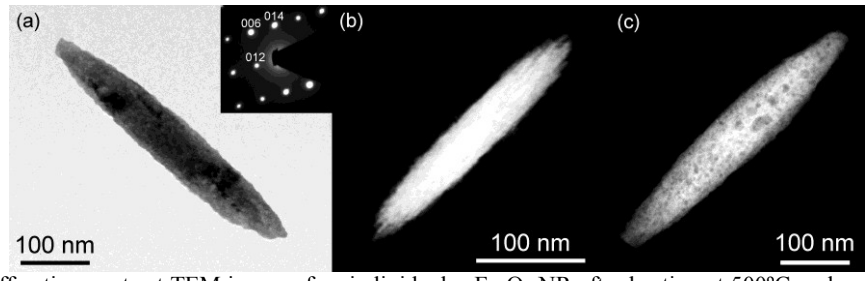

Figure 4 (a) BF diffraction contrast TEM image of an individual α-Fe_2O_3 NR after heating at 500ºC under an H_2 atmosphere of 5 mbar for 5 hours, as identified by SAED (inset, indexed). (b,c) HAADF images of α-Fe_2O_3 NRs examined (b) before and (c) after heating at 500ºC under an H_2 atmosphere of 5 mbar for 5 hours.

the localised development of Fe_3O_4 NPs on the side and tip of α-Fe_2O_3 NRs (Figures 2 and 3, respectively). It is likely that focusing the 300keV electron beam, during imaging (Figures 2 & 3) contributed to the development of the Fe_3O_4 NPs in this low pressure H_2 environment. In Figures 2b-i, the electron beam was converged on an area slightly larger than the field of view, which included the location of the newly formed NPs (Figure 2j, arrowed). Likewise, formation of the Fe_3O_4 NP on the tip of the α-Fe_2O_3 NR (Figure 3c) occurred during high resolution imaging. Further, the surface of the α-Fe_2O_3 NR shown in Figure 2j became noticeably eroded. Hence, the high current density of the electron beam acted to destabilise the α-Fe_2O_3 NR surface, allowing oxygen to react with H_2 and form water, leaving an oxygen deficiency in the α-Fe_2O_3 NR surface, whilst remaining unstable iron and oxygen supplied the growth of Fe_3O_4 NPs.

Considering the relationship between the orientation of the α-Fe_2O_3 NRs and the growth of the initial Fe_3O_4 NPs, Figures 2 and 3 illustrate the formation of Fe_3O_4 NPs on the side and tip of α-Fe_2O_3 NRs, respectively. Closer examination reveals the growth interface of the tip Fe_3O_4 NP to be parallel to the major axis of the α-Fe_2O_3 NR (Figure 3c, inset), and hence, in both cases, the Fe_3O_4 NPs grow on surfaces parallel to the α-Fe_2O_3 <006> direction. Elemental supply to developing Fe_3O_4 NPs through an interface parallel to the α-Fe_2O_3 c-axis reinforces the notion that α-Fe_2O_3 {006} planes are favourable for oxygen diffusion during the thermal reduction of α-Fe_2O_3 NRs to Fe_3O_4 NRs. The α-Fe_2O_3 {006} or Fe_3O_4 {111} planes may become unstable and collapse during oxygen diffusion, resulting in defects.

In summary, fine details of the reduction of α-Fe_2O_3 NRs to Fe_3O_4 NRs during *in situ* XRD were examined. ETEM experiment provided evidence to support a model for oxygen migration along favoured α-Fe_2O_3 lattice planes during templated thermal reduction of α-Fe_2O_3 NRs to Fe_3O_4 NRs.

References

[1] Bate G, 1991 *J. Magn. Magn. Mater.***100**, 413.
[2] Mornet S, Vasseur S, Grasset F, Duguet E, 2004 *J. Mater. Chem.* **14**, 2161-2175.
[3] Itoh H and Sugimoto T, 2003 *J. Colloid Interface Sci.* **265,** 283-295.
[4] Almeida T P, Fay M W, Zhu Y Q and Brown P D, 2010 *Nanoscale* **2**, 2390–2399.
[5] Hansen T W, Wagner J B and Dunin-Borkowski R E, 2010, *Materials Science and Technology* **26,** 1338-1344.
[6] Boyes, E D, Gai, P L, 1997 *Ultramicroscopy* **67,** 219-232.
[7] Watanabey Y, Takemuraz S, Kashiwayaz Y and Ishii, K, 1996, *J. Phys. D: Appl. Phys.* **29**, 8–13.
[8] Suber L, Fiorani D, Imperatori P, Foglia S, Montone A and Zysler, R, 1999, *NanoStruct. Mater.* **11**, 797-803.